Journal of Earthquake Engineering, 14:80–101, 2010

ISSN: 1363-2469 print / 1559-808X online
DOI: 10.1080/13632460902977474

Taylor & Francis
Taylor & Francis Group

Seismic Assessment of Masonry "Gaioleiro" Buildings in Lisbon, Portugal

NUNO MENDES and PAULO B. LOURENÇO

Department of Civil Engineering, ISISE, University of Minho, Guimarães, Portugal

This article presents a numerical study for the seismic assessment of a Portuguese building masonry typology - "Gaioleiro." Numerical analysis was performed using a finite element model calibrated with experimental results obtained in 1:3 reduced scale tests carried out in the LNEC 3D shaking table. Nonlinear dynamic analysis with time integration and pushover analysis are carried out.

Using nonlinear dynamic analysis it was verified that the buildings of "Gaioleiro" type with appropriate floor-wall connections are in the limit of their loading capacity. The pushover analyses performed in this study were incapable of simulating correctly the damage of the structure under seismic action.

Keywords "Gaioleiro"; Buildings; Masonry; Earthquake; Seismic Assessment; Nonlinear Time History Analysis; Pushover Analysis

1. Introduction

Earthquakes are known by their catastrophic effects. Information from the United Nations reveals that the percentage of deaths originated by phenomena of seismologic character was 26% of the total number of casualties caused by natural disasters, with an estimate of more than fourteen million of victims since 1755 [Barbat *et al.*, 2006].

It is not possible to act on the seismic hazard, meaning that mitigation of the seismic risk can only be made through reduction of the vulnerability. The study of seismic vulnerability can address new and existing buildings. Enough scientific knowledge seems to be available to design structures with appropriate seismic safety. The difficulty can be to guarantee that the regulations are fulfilled and that the execution follows correctly the structure design [Oliveira, 2004].

The study of ancient buildings has been, in general, limited. Only in the past decades has this issue been taken into account due to the increasing interest in the conservation of the built heritage and the awareness that life and property must be preserved. With respect to the built heritage, masonry buildings represent a major part of the stock and they were often non engineered or not designed with reference to any particular code [Benedetti *et al.*, 1998].

In Portugal, the Portuguese Society of Earthquake Engineering (SPES) and the Portuguese Association of Companies for Conservation and Restoration of the Architectural Heritage (GECoRPA) elaborated a reduction program of the seismic vulnerability of the building stock [SPES and GEOeRPA, 2001]. The objective is to evaluate and reduce the seismic vulnerability through seismic retrofitting of the building

Received 16 July 2008; accepted 10 April 2009.

Address correspondence to Nuno Mendes, Department of Civil Engineering, University of Minho, Guimarães Portugal; E-mail: nunomendes@civil.uminho.pt

stock, similarly to programs executed or proposed in others seismic countries (USA, New Zealand, Japan, Italy, and Turkey). This program was prepared taking into consideration the most recent methods of large scale seismic assessment. For this purpose, a representative building of a certain typology should be selected and, through the analysis of the individual representative building, the seismic performance of the typology is estimated.

The present study is focused on this sought reduction of the seismic vulnerability of the building stock, aiming at evaluating the seismic performance of the "gaioleiro" buildings (Fig. 1). This building typology developed between the mid 19th century and beginning of the 20th century, mainly in the city of Lisbon, still remains much in use nowadays. These buildings characterize a transition period from the anti-seismic practices used in the "pombalino" buildings originated after the earthquake of 1755 (see, e.g., Ramos and Lourenço, 2004), and the modern reinforced concrete frame buildings. The "gaioleiro" buildings are, usually, four or five stories high, with masonry walls and timber floors and roof. The external walls are, usually, in rubble masonry with lime mortar [Pinho, 2000]. In the urban areas these buildings are usually semi-detached and belong to a block of buildings. Although it is not an objective of this article, pounding can be taken in account when the adjacent buildings present different heights or the separation distance is not large enough to accommodate the displacements [Gulkan *et al*., 2002; Viviane, 2007]. It is noted the "block" effect is usually beneficial and provides higher strength of the building, as shown in Ramos and Lourenço [2004].

In the seismic assessment of the "gaioleiro" buildings, nonlinear dynamic and static analyses were performed. The numerical model was calibrated with experimental results obtained in 1:3 reduced scale tests including only the dead load. Subsequently, after calibration, the model was changed and the live load prescribed in the code was added. Furthermore, in the experimental tests the seismic action was defined according the Portuguese Code [RSA, 1984] and in the numerical analyses the Eurocode 8 [EN 1998-1, 2004] and the Portuguese National Annex were used. This procedure is justified as the aim of the work is to evaluate the seismic performance of the "gaioleiro" buildings under the present safety requirements.

2. Experimental Program

The National Laboratory of Civil Engineering, Lisbon (LNEC), carried out a set of shaking table tests with the purpose of evaluating the seismic performance of the "gaioleiro" buildings, before and after strengthening [Candeias *et al.*, 2004]. In the test

FIGURE 1 Examples of "gaioleiro" buildings, Lisbon, Portugal.

program, a prototype of an isolated building was defined, constituted by four stories with an interstory height of 3.60 m, 2 opposite facades with a percentage of openings equal to 28.6% of the facade area, 2 opposite gable walls (with no openings), timber floors, and a gable roof.

Due to the size and payload of the shaking table, the experimental model was built using a 1:3 reduced scale, taking in account Cauchy's law of similitude (Table 1). The geometric properties of the experimental model result directly from the application of the scale factor to the prototype, resulting in a model with 3.15 m wide, 4.8 m deep, and 0.15 m of wall thickness (Fig. 2). The experimental model only has the top ceiling, due to difficulties in reproducing the gable roof at reduced scale.

TABLE 1 Scale factors of the cauchy similitude [Carvalho, 1998] (where $_p$ and $_m$ designate prototype and experimental model, respectively)

Parameter	Symbol	Scale factor
Length	L	$L_p/L_m=\lambda=3$
Young's Modulus	E	$E_p/E_m=\lambda=1$
Specific mass	ρ	$\rho_p/\rho_m=\lambda=1$
Area	A	$A_p/A_m=\lambda^2=9$
Volume	V	$V_p/V_m=\lambda^3=27$
Mass	m	$m_p/m_m=\lambda^3=27$
Displacement	d	$d_p/d_m=\lambda=3$
Velocity	v	$v_p/v_m=\lambda=1$
Acceleration	a	$a_p/a_m=\lambda^{-1}=1/3$
Weight	W	$W_p/W_m=\lambda^3=27$
Force	F	$F_p/F_m=\lambda^2=9$
Moment	M	$M_p/M_m=\lambda^3=27$
Stress	σ	$\sigma_p/\sigma_m=\lambda=1$
Strain	ε	$\varepsilon_p/\varepsilon_m=\lambda=1$
Time	t	$t_p/t_m=\lambda=3$
Frequency	f	$f_p/f_m=\lambda^{-1}=1/3$

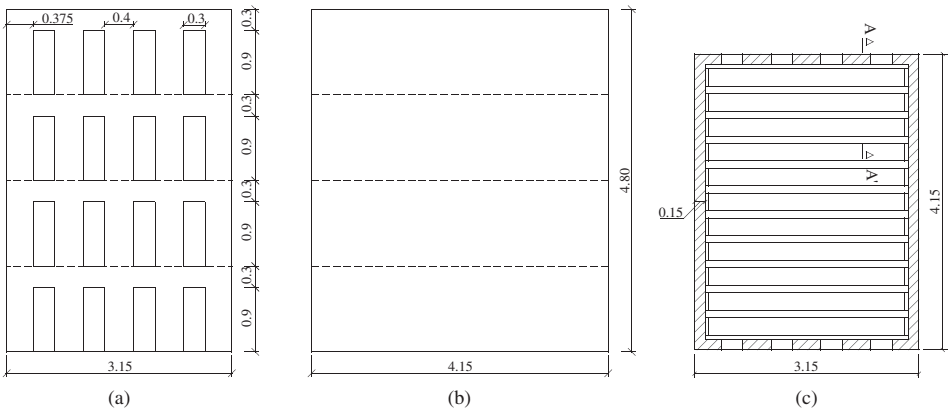

FIGURE 2 Experimental model (dimensions in meters): (a) facade; (b) side (gable) wall; (c) plan.

The external walls, originally built in poor quality rubble masonry with lime mortar, were replaced by a self compacting bentonite-lime concrete, studied to reproduce the mechanical characteristics of the original masonry walls, namely with respect to compressive strength, tensile strength, and Young's modulus.

In the construction of the timber floors, medium-density fiberboard (MDF) panels connected to a set of timber joists oriented in the direction of the shortest span were used. The panels were cut in rectangles of 0.57 m $\times$ 0.105 m and stapled to the joists, keeping a joint of about 1 mm for separating the panels. The purpose was to simulate flexible floors with very limited diaphragmatic action (Fig. 3).

As mentioned above, a model without strengthening and models with different techniques of strengthening were tested [Candeias *et al.*, 2004]. In the present study, reference is made to Model 0 (without strengthening and weak wall-to-floor connection) and Model 1 (strong wall-to-floor connection). In the wall-to-floor connection, steel connectors and fiber strips glued with epoxy resins were used. The strong connection was made only in the 3rd and 4th floors near the piers (facades) and on the supports of the joists (gable walls). Figures 4a and 4b show Model 0 and the details of the connections used in Model 1, respectively.

The dynamic tests were performed on the LNEC triaxial shaking table by imposing time series of artificial accelerograms compatible with the design response spectrum defined by the present Portuguese code [RSA, 1984] for zone A and very stiff soil. The time series were imposed with increasing amplitude and in two uncorrelated orthogonal directions. Before the beginning of the tests and after each time series, the dynamic properties of the models were characterized [Candeias *et al.*, 2004]. The time series in the two orthogonal directions are uncorrelated and should present the same *PGA*. However, due to experimental difficulties in the tests, the *PGA* in the longitudinal direction is about 1.4 times of *PGA* in the transversal direction.

Figures 5a and 5b present the damage details of the Model 0 and Model 1 after testing, respectively.

3. Definition and Calibration of the Numerical Model

3.1. Definition of the Numerical Model

The numerical model of the building was prepared using the Finite Element (FE) software DIANA [2005], by using shell elements for the simulation of the walls and three-dimensional beam elements for the timber joists, all based on the theory of Mindlin-Reissner. In the modeling of the floors, shell elements were also used with the purpose of

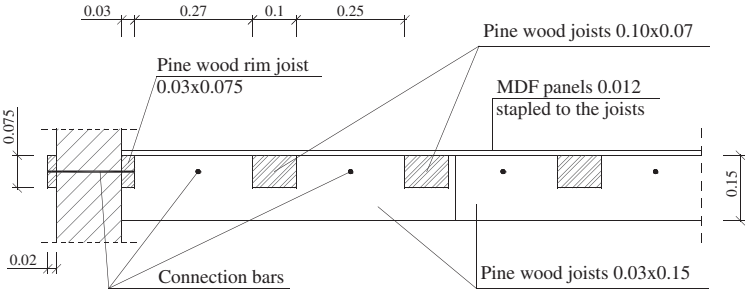

FIGURE 3 Floors (Sec. AA' from Fig. 2).

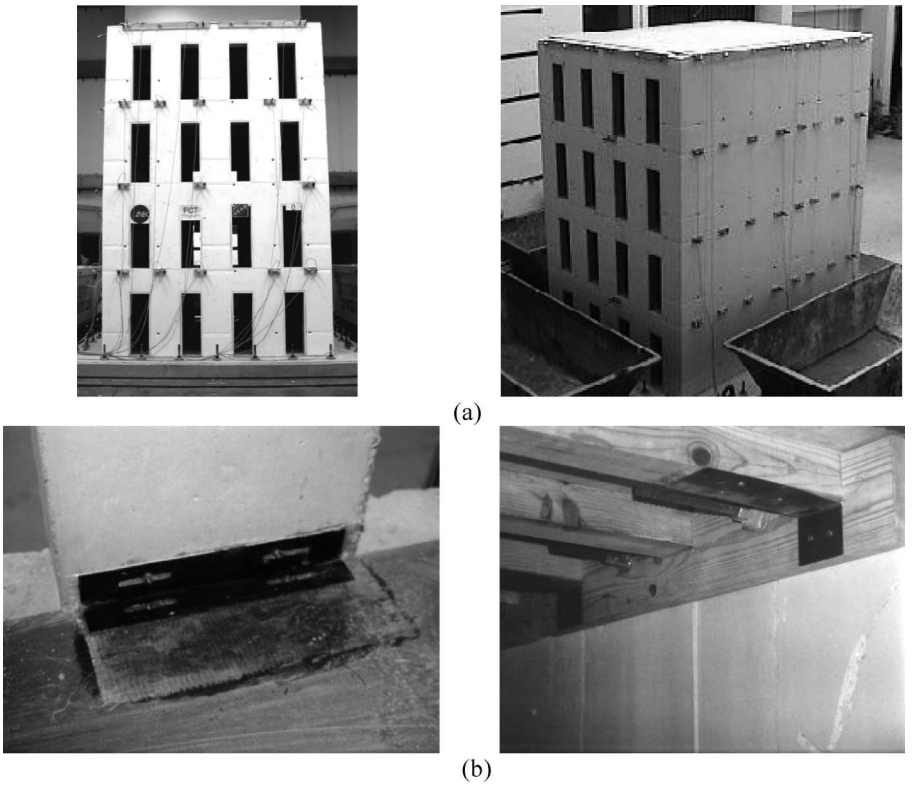

FIGURE 4 Experimental models: (a) Model 0; (b) details of the Model 1 wall-to-floor connection.

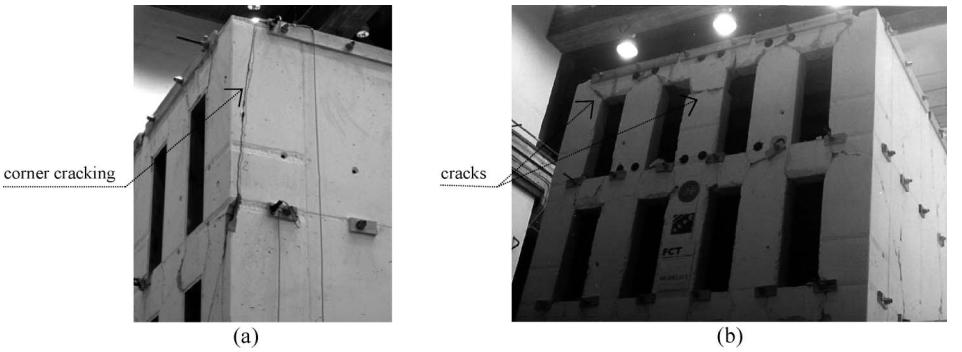

FIGURE 5 Cracks patterns: (a) Model 0; (b) Model 1.

simulating the in plane deformability (Fig. 6). In the supports, only the translation degrees of freedom in the base were restrained. The full model involves 5816 elements (1080 beam elements and 4736 shell elements) with 15,176 nodes, resulting in 75,880 degrees of freedom (DOF).

The behavior of the connection between the floors and the walls is unknown, as no measurements were taken for a possible separation and the eigenmodes in the longitudinal direction were difficult to characterize due to presence of noise. Thus,

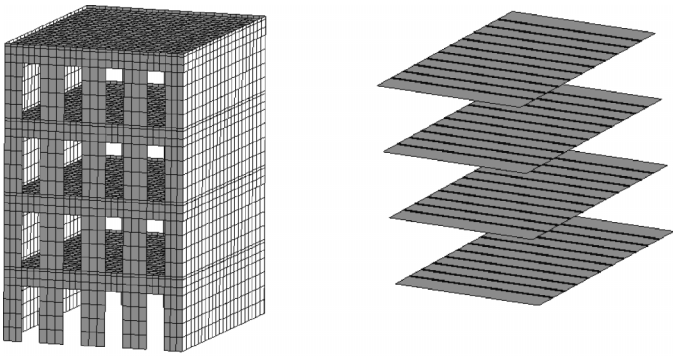

FIGURE 6 Numerical model: (a) global view of the finite element mesh; (b) floor elements.

preliminary numerical analyses were made with the purpose of validating the assumption used for the facade-wall connection.

Preliminary numerical analyses were carried out using the artificial accelerograms used in the tests, with the lowest peak ground acceleration. It is noted that the behavior of the Models 0 and 1 are similar for low acceleration amplitudes ($PGA_{longitudinal}$ = 0.9 m/s^2), and the response is basically linear elastic. The following extreme hypotheses for the connection of the facades to the floors were adopted: (a) the translation degrees of freedom are fully tied; (b) there is no horizontal connection between walls and timber floors.

After an iterative process for proper selection of the material properties, it was concluded that the hypothesis of a model with full translational wall-floor connection is the most appropriate. Figure 7 shows the behavior at the top of the structure without and with connection of the floors to the walls. It is noted that in the hypothesis of model without wall-floor connection the facades vibrate almost independently from the remaining structure. This behavior does not hold in the hypothesis of the model with wall-floor connection, which is in correspondence with the observed experimental model behavior.

As full wall-floor connection better approaches the linear behavior of the structure, this model was adopted for calibration of the dynamic characteristics of the structure: frequencies and modes of vibration.

3.2. Calibration of the Numerical Model

Calibration of the numerical model was accomplished with the methodology proposed by Douglas-Reid [1982], in which the frequency i of the structure f_i^D can be estimated by means of:

$$f_i^D(X_1, X_2, ..., X_N) = C_i + \sum_{k=1}^{N} \left[A_{ik}X_k + B_{ik}X_k^2\right], \quad (1)$$

where $X_k(k=1,2,\ldots,N)$ are the variables to calibrate and A_{ik}, B_{ik}, and C_i are constants.

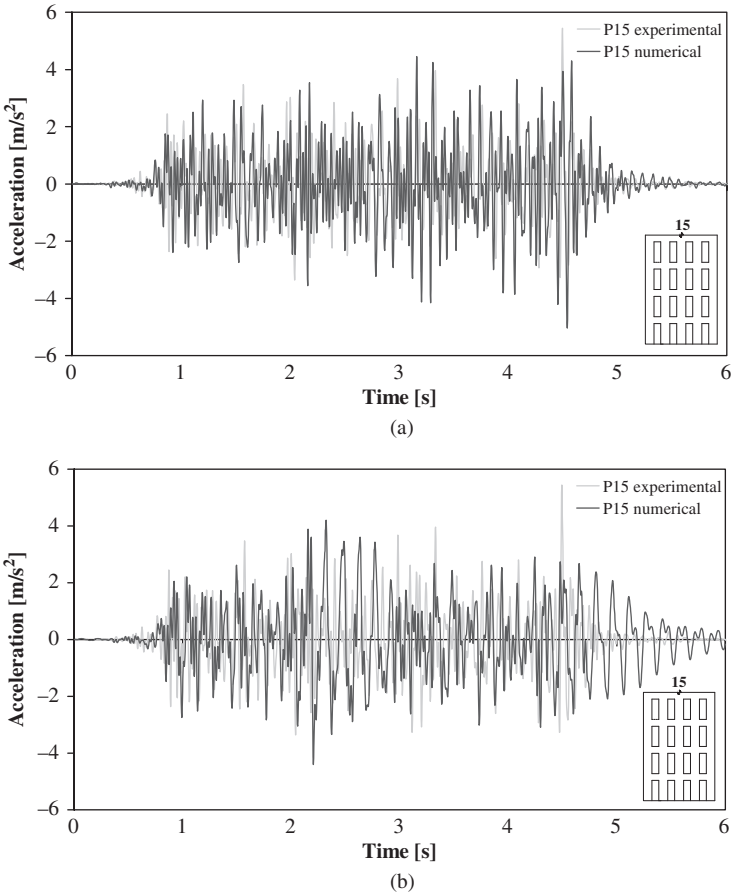

FIGURE 7 Acceleration at facade top: (a) with wall-to-floor connection (all translation degrees of freedom tied); (b) without wall-to-floor connection (vertical translation degrees of freedom tied).

The (2*N*+1) constants can be obtained by the following system of equations:

$$
\begin{aligned}
f_i^D\left(X_1^B, X_2^B, ..., X_N^B\right) &= f_i^C\left(X_1^B, X_2^B, ..., X_N^B\right) \\
f_i^D\left(X_1^L, X_2^B, ..., X_N^B\right) &= f_i^C\left(X_1^L, X_2^B, ..., X_N^B\right) \\
f_i^D\left(X_1^U, X_2^B, ..., X_N^B\right) &= f_i^C\left(X_1^U, X_2^B, ..., X_N^B\right) \\
&\ldots \\
f_i^D\left(X_1^B, X_2^B, ..., X_N^L\right) &= f_i^C\left(X_1^B, X_2^B, ..., X_N^L\right) \\
f_i^D\left(X_1^B, X_2^B, ..., X_N^U\right) &= f_i^C\left(X_1^B, X_2^B, ..., X_N^U\right),
\end{aligned}
\tag{2}
$$

where f_i^C are the frequencies calculated by means of the numerical model, $X_k^B(k=1,2,\ldots,N)$ are the base values of the variables, and $X_k^U(k=1,2,\ldots,N)$ and $X_k^L(k=1,2,\ldots,N)$ are their respective upper limit and lower limit values.

After calculating the constants, an optimization process of the calibration variables is used, with the purpose of minimizing the following equation:

$$J = \sum_{i=1}^{m} w_i \varepsilon_i^2 \tag{3}$$

with

$$\varepsilon_i = f_i^{EMA} - f_i^D (X_1, X_2, ..., X_N) \tag{4}$$

where f_i^{EMA} are the experimental values of the frequencies and w_i are the weight factored.

In the present study, the numerical model was calibrated using the first two natural frequencies obtained in the modal identification (first translational mode and first torsional mode), defining as variables to calibrate the Young's modulus of the different materials. After an optimization process carried out using the software GAMS [1998], the optimal values of the Young's modulus were obtained (Table 2). It is noted that the low value found for the Young's modulus of the MDF panels is due to the floors arrangement (open joints). Table 3 presents the values of the frequencies after calibration.

It is known that this building typology presents physical nonlinear behavior under acceleration time series with larger values of *PGA* ($PGA > 0.9$ m/s^2). Thus, the behavior of the structure under the highest acceleration series of the tests ($PGA = 9.75$ m/s^2) was studied with the purpose of obtaining a crack pattern similar to the one obtained in the tests. In these analyses only the physical nonlinear behavior of the masonry walls was considered.

For this purpose, reasonable nonlinear properties were initially assumed for the masonry material with adjustments in the fracture energies so that the crack pattern presented in Fig. 8 could be found. It is verified that the numerical model is able to simulate correctly the behavior of the experimental model with appropriate wall-floor connection (Model 1), in which damage concentration at the 4th floor is highlighted.

The physical nonlinear behavior of the masonry walls was simulated using the Total Strain Crack Model detailed in [DIANA, 2005]. This includes a parabolic stress-strain relation for compression, where the compressive strength, f_c, is equal to 0.8 N/mm^2 and the respectively fracture energy, G_c, is equal to 1.25 N/mm. In tension, an exponential tension-softening

TABLE 2 Linear elastic properties

	Young's modulus [N/mm^2]	Poisson's ratio	Specific mass [Kg/m^3]
Walls	779	0.2	1910
MDF panels	240	0.3	760
Wood joist	12000	0.3	580

TABLE 3 Numerical frequencies after calibration

	1st Transversal mode	1st Distortion mode
Numerical [Hz]	4.80	9.23
Experimental [Hz]	4.73	9.09
Error [%]	1.48	1.54

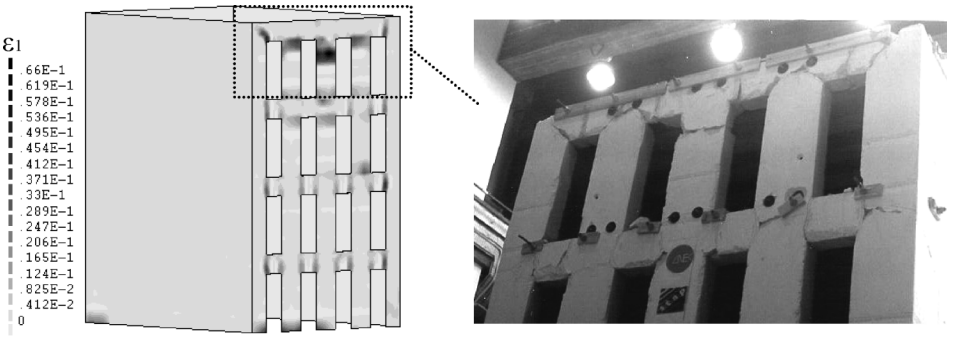

FIGURE 8 Damage after testing in the model: (a) numerical; (b) experimental (Model 1). (ε_1 is the principal tensile strain, which is an indicator of crack width).

diagram was adopted, where the tensile strength, f_t, is equal to 0.125 N/mm^2 and the fracture energy, G_t, is equal to 0.125 N/mm. The crack bandwidth, h, was determined as a function of the finite element area, A (Eq. (5)). In terms of shear behavior, a constant shear retention factor equal to 0.01 was adopted. Figure 9 presents the hysteretic behavior adopted for the masonry.

$$h = \sqrt{A} \tag{5}$$

Damping, $\underline{C}$, was simulated according to Rayleigh viscous damping [Chopra, 2000], which is a linear combination of the mass, $\underline{M}$, and of stiffness, $\underline{K}$, matrices (Eq. (6)). Constants α (2.18) and β (0.00044) were determinated from the results obtained in the dynamic identification tests (Table 4). In the damping identification, a curve fiting of the Frequency Response Function (FRF) for a Single Degree of Fredom was used.

$$\underline{C} = \alpha \underline{M} + \beta \underline{K} \tag{6}$$

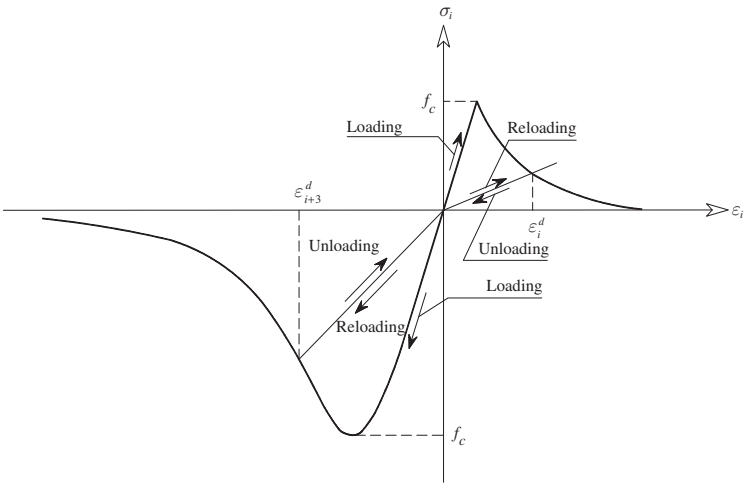

FIGURE 9 Adopted hysteretic behavior of masonry.

TABLE 4 Experimental modal damping ratio

	Frequency [Hz]	Modal damping ratio [%]
1st Translational mode	4.80	4.3
1st Torsional mode	9.23	2.5

3.3. Incorporation of Live Load

The experimental model only considered the self-weight of the walls and of the floors. In the calibrated numerical model, all code loads are now considered, including the self weight of the partition walls, cladding and roof, and the quasi-permanent part of the live load. Figure 10 presents four mode shapes in the transversal and longitudinal directions of the calibrated model with additional mass.

Using the calibrated model with the code masses, a safety analysis is now made using nonlinear time history analysis (Sec. 4) and pushover analysis (Sec. 5).

4. Nonlinear Time History Analyses

4.1. Seismic Action

The horizontal seismic action is described by two orthogonal and independent components, represented by the same response spectrum. Three earthquakes were used, composed of two uncorrelated artificial accelerograms (Earthquake 1, 2, and 3). The artificial accelerograms are compatible with the elastic response spectrum (Type 1) defined by Eurocode 8 [EN 1998-1, 2004], for the zone of Lisbon, with a damping ratio ξ equal to 5% and a type A soil (rock). The accelerograms were generated using the software SIMQKE_GR [Gelfi, 2006], with a baseline correction using SeismoSignal [Seismosoft, 2004]. Due to the fact that nonlinear dynamic analyses are very time

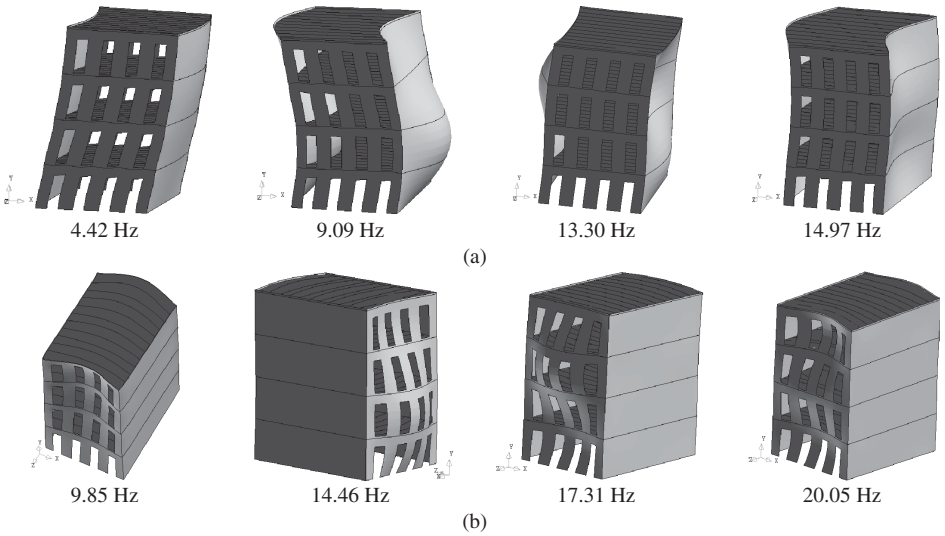

FIGURE 10 Calculated mode shapes in the: (a) transversal direction; (b) longitudinal direction.

consuming and the response spectrum of Type 1 (interplate earthquake) is usually more stringent for Lisbon area and for the type of structures being considered, only one type of earthquake was considered.

It is noted that a response spectrum is a spectral representation of the peak response of single degree of freedom system with a given common damping ζ and natural periods T_n (varying from a minimum value up to a maximum value) to a given seismic input motion. Thus, for a given input motion, it is possible to obtain several response spectra associated with different values of damping adopted. The process of generating time histories compatible with the input for a response spectrum is therefore independent of the damping considered. Concerning the codes, Eurocode 8 clearly defines that the artificial accelerograms shall be generated so as to match the elastic response spectra for 5% viscous damping.

Using the 1:3 reduced scale, the accelerograms have a total duration of 6 s, from which 3.33 s correspond to the intense phase, and a *PGA* equal to 4.51 m/s^2.

4.2. Analysis Tools

Nonlinear time history analysis on masonry structures is complex and takes a long time for the model considered. In opposition to the typical framed concrete structures, where it is easy to identify the yield hinges, masonry buildings have distributed cracking around the structure, which features opening, closing and reopening, due to the low value of the tensile strength.

The quasi-brittle masonry behavior in tension introduces numerical noise, due to the fast transition from linear elastic behavior to a fully cracked state involving an almost zero stiffness. The quasi-instantaneous changes in the displacement field tend to originate the propagation of high frequency spurious vibrations [Cervera *et al.*, 1995]. Therefore, it is important to adopt the Hilber-Hughes-Taylor time integration method [DIANA, 2005] (also called the α method), which was used here with α equal to –0.1. With this method it is possible to introduce numerical dissipation without degrading the accuracy. The Hilber-Hughes-Taylor method uses the same finite difference equations as the Newmark method with:

$$\gamma = \frac{1}{2}(1 - 2\alpha) \tag{7}$$

and

$$\beta = \frac{1}{4}(1 - \alpha)^2. \tag{8}$$

For $\alpha = 0$ the method reduces to the Newmark method. For $-1/3 = \alpha = 1/2$ the scheme is second-order accurate and unconditionally stable. Decreasing α means increasing the numerical damping, and the adopted damping is low for low-frequency modes and high for the high-frequencies modes.

The time step Δt was determined using Eq. (9), in order to account for the lowest period with relevance in the structural behavior T_i, with an error lower than 5%. It was assumed that T_i was equal to 0.025 s [Mendes and Lourenço, 2008], meaning that Δt is equal to 0.00125 s.

$$\Delta t = \frac{1}{20} T_i \tag{9}$$

Concerning the iteration method, the regular Newton-Raphson method, in which the tangential stiffness is set up before each iteration, was used. In the equilibrium

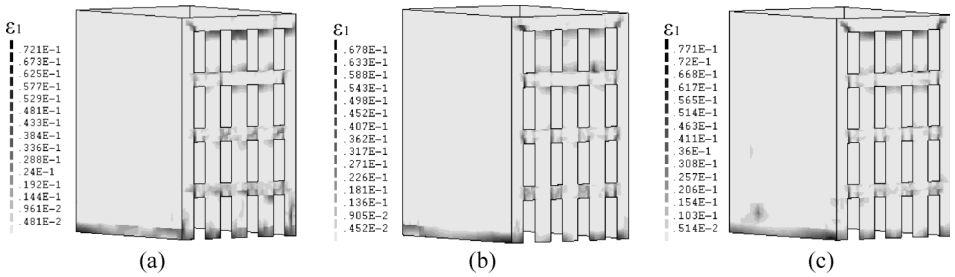

FIGURE 11 Tensile principal stains (outside surface): (a) earthquake 1; (b) earthquake 2; (c) earthquake 3.

iteration process, a convergence criterion based on the internal energy and a tolerance equal to 10^{-3} was used.

4.3. Results

In the numerical modeling the time series were applied directly with the prescribed code value. It is noted that in the experimental testing the time series were imposed with increasing amplitude and this can influence the final results, although the final crack pattern did not change significantly.

Figure 11 presents the maximum values of the tensile principal strains ε_1 for the three earthquake records. The results indicate that the facades at the 4th floor and the base of the structure are the zones of larger damage concentration, being the high level of damage in the 4th floor's piers highlighted.

The relation between the "seismic coefficient" α_h defined by Eq. (10) and the horizontal displacement at the top of the structure was plotted. The envelopes of these relations, for the different earthquakes and directions, are presented in Figs. 12 and 13. It is observed that the maximum values of α_h are about 0.2 and 0.65 in the transversal and longitudinal directions, respectively (approximately a relation 100% longitudinal "+" 31% transversal).

$$\alpha_h = \frac{\sum Horizontal\,forces}{Self\ weight\ of\ the\ structure} \tag{10}$$

5. Nonlinear Static (Pushover) Analyses

5.1. Capacity Curves

In the pushover analysis the capacity curves was considered by increasing a set of lateral loads applied to the structure in two independent directions. Two vertical distributions of lateral loads were used: (a) uniform pattern, based on lateral forces proportional to mass regardless of elevation – uniform response acceleration; (b) modal pattern, proportional to forces consistent with the 1st mode shape in the applied direction. In an attempt to explore the pushover analyses proportional to the 1st mode shape, an additional adaptive pushover analysis was also carried out.

In the pushover analysis physical and geometrical nonlinear behavior was considered, even if it is expected that the geometrical nonlinear effects have minor influence in the maximum load.

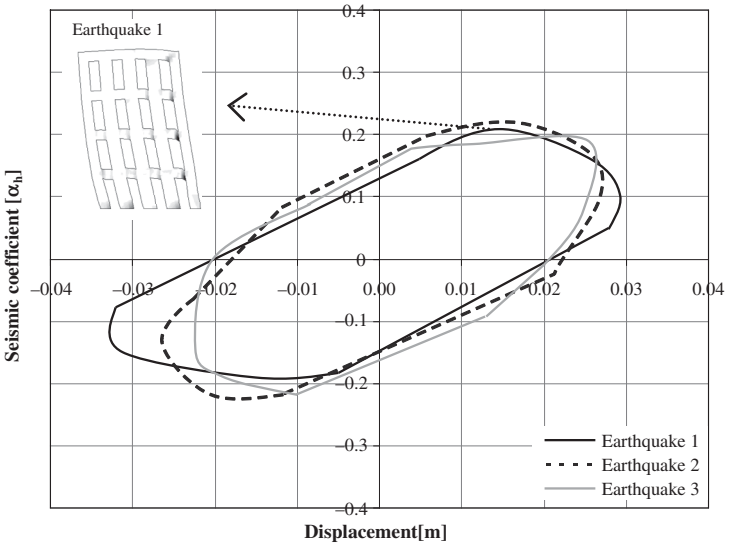

FIGURE 12 Envelope of the relation between the horizontal displacement (4th floor) and the seismic coefficient in the transversal direction.

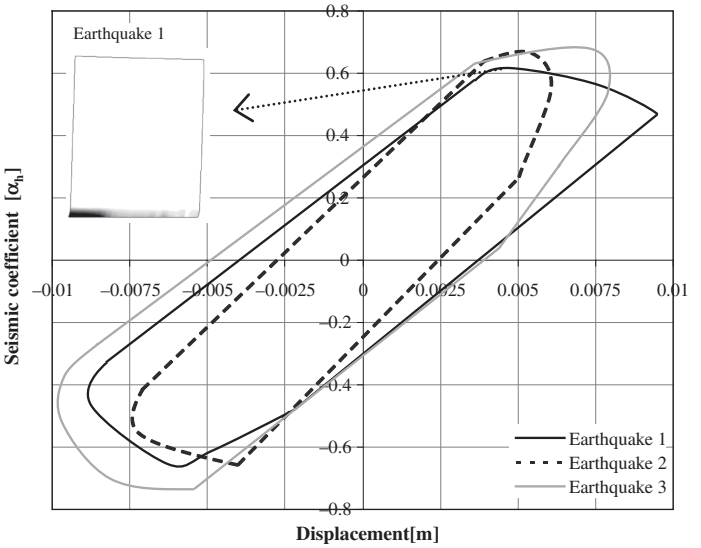

FIGURE 13 Envelope of the relation between the horizontal displacement (4th floor) and the seismic coefficient in the longitudinal direction.

For the solution procedure, the regular Newton-Raphson method, the line search algorithm and the arc-length control were used.

5.2. Pushover Analysis Proportional to the Mass

The capacity curves of the pushover analyses proportional to the mass show that the maximum seismic coefficients are higher than the dynamic analysis (about 24%) (Fig. 14).

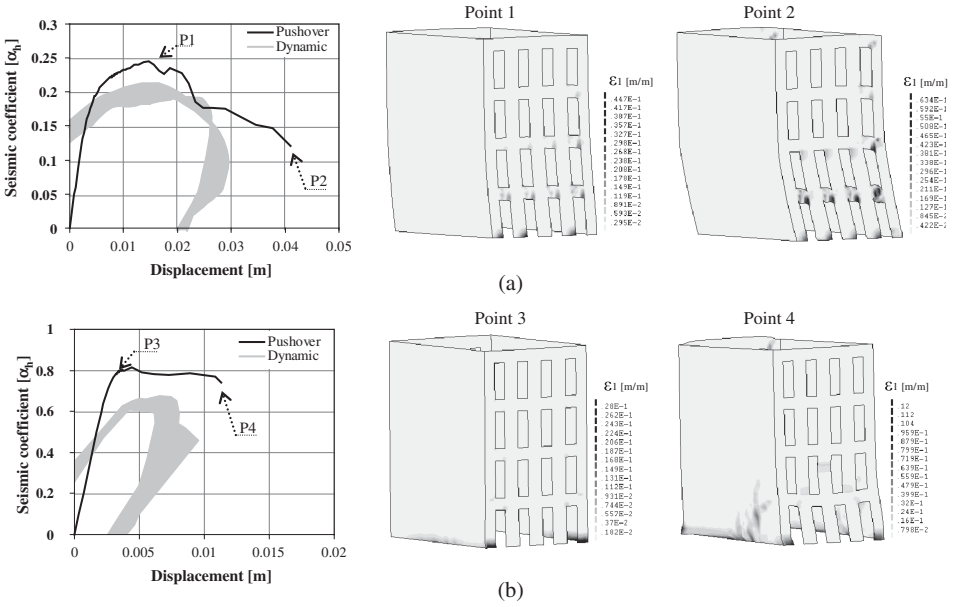

FIGURE 14 Capacity curves and tensile principal strains of the pushover analysis proportional to the mass in the: (a) transversal direction; (b) longitudinal direction.

In the pushover analysis proportional to the mass, the damage concentration only appears at the lower zone of the structure (Fig. 14). It is noted that in the dynamic analysis the damage concentrates at the 4th floor (facades) and at the base (Fig. 11). Thus, this pushover analysis does not simulate correctly the performance of "gaioleiro" buildings under seismic load.

5.3. Pushover Analysis Proportional to the 1st Mode Shape

The capacity curves of the pushover analysis proportional to the 1st mode (in the applied direction) show that the maximum seismic coefficients approach the dynamic analysis. The crack patterns only provide in plane damage, which is not in agreement with the out-of-plane mechanism found in the time integration analysis and shaking table test (Fig. 15). Hence, the damage at the upper stories must have a significant contribution from the higher modes, including the local modes of the piers.

5.4. Adaptive Pushover Analysis

In the adaptive pushover analysis the lateral loads, proportional to the 1st mode shape in the applied direction were updated as a function of the existing damage. Here, the aim is to understand how the update of the external load vector can influence the structure response.

The analysis was done in four phases and after each phase the new modal shape was calculated by using the tangential stiffness matrix (Eq. (11)), allowing the updating of the load distribution as function of the damage,

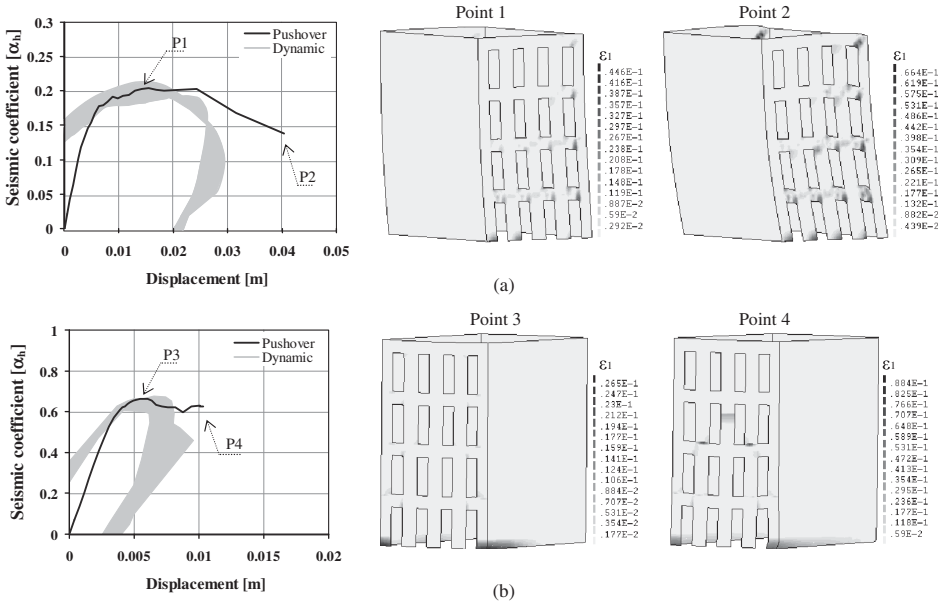

FIGURE 15 Capacity curves and tensile principal strains of the pushover analysis proportional to the 1st mode shape in the: (a) transversal direction; (b) longitudinal direction.

$$\left(\underline{k_t} - w_i^2 \underline{M}\right) \underline{\phi_i} = 0, \tag{11}$$

where

$\underline{k_t}$ is the tangential stiffness matrix;
w_i is the angular frequency;
$\underline{M}$ is the mass matrix;
$\underline{\phi_i}$ is the mode shape vector.

The adaptive pushover analysis (Fig. 16a) in the transversal direction presents a decrease of the maximum seismic coefficient (about 21% of the maximum seismic coefficient of the pushover analysis proportional to the 1st mode in the corresponding direction). Since the lintels crack progressively, the update of the load distribution has influence in the structure behavior. The crack pattern (Fig. 17a) presents damage concentration in the lintels and at the base.

In the longitudinal direction the adaptive pushover analysis (Figs. 16b and 17b) provides the same behavior of the pushover analysis proportional to the 1st mode in the corresponding direction. In fact, in the longitudinal direction the structure is very stiff, when compared to the transversal direction. Up to the maximum seismic coefficient the damage is almost non-existent and after reaching this value, the structure presents a brittle behavior. So, in this direction the update of the load distribution does not have influence in the response.

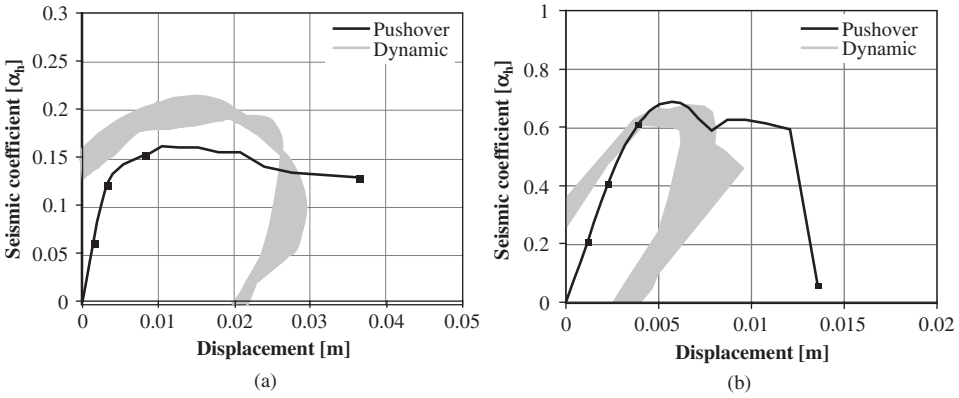

FIGURE 16 Capacity curves of the adaptive pushover analysis in the: (a) transversal direction; (b) longitudinal direction (the points delimit the phases).

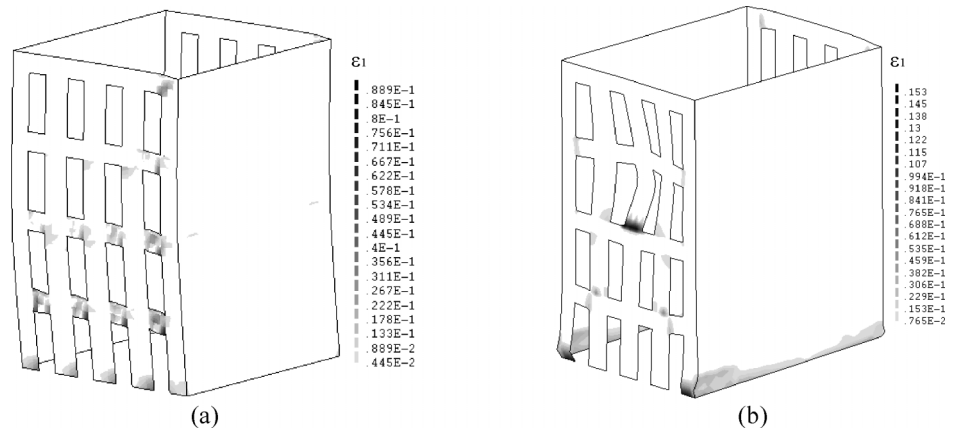

FIGURE 17 Tensile principal strains (outside surface) of the adaptive pushover analysis in the: (a) transversal direction; (b) longitudinal direction.

6. Discussion About the Collapse Mechanisms Found

The "gaioleiro" buildings under seismic load present a damage concentration at the 4th floor (facades) and at the base (Fig. 11), being this result a combination of in-plane and out-of-plane actions. The damage represents the typical failure mechanism of masonry buildings (Fig. 18): (a) cracking around the corners of the openings; (b) out-of-plane collapse (4th floor's piers). The different pushover analyses performed in this work could not simulate correctly the damage of the structure.

The analysis of the collapse mechanism in terms of displacements at floor levels (or drifts) does not characterize the observed crack patterns. In case of the time integration analysis, the maximum out-of-plane displacement is equal to 10 mm and a correlation between the out-of-plane drift and damage would indicate a maximum damage between the ground and the first floor level (Fig. 19). Thus, in opposition to framed concrete structures, the evaluation of results at the floor levels is not enough to identify correctly the zones of largest damage of masonry buildings.

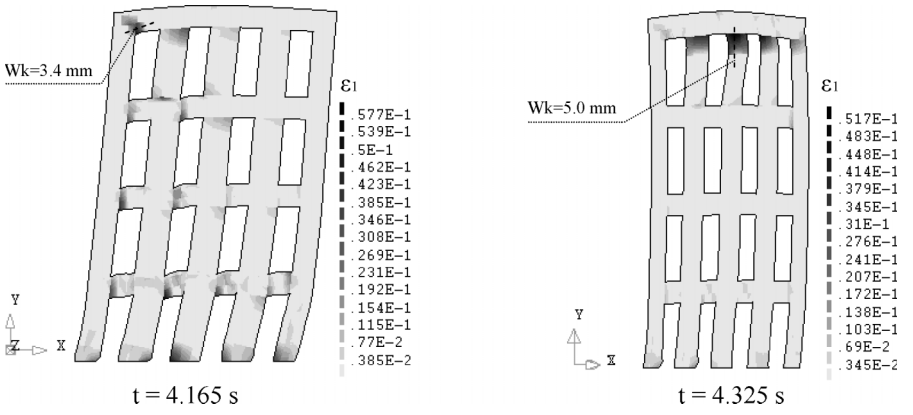

FIGURE 18 Details of the earthquake 1 damage (w_k is the crack width obtained by integrating the strains).

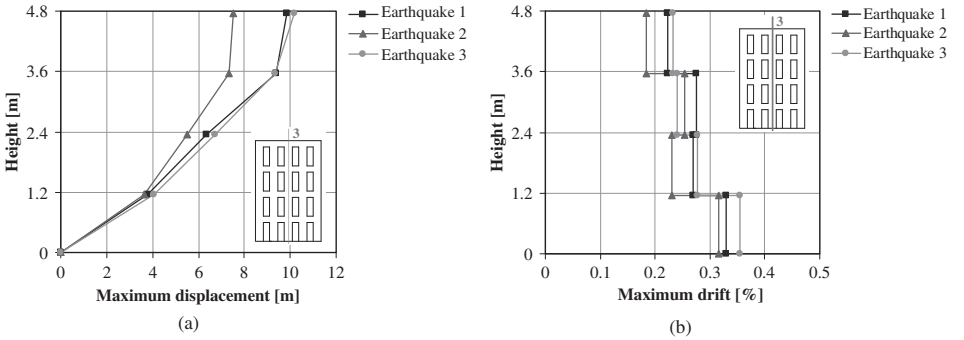

FIGURE 19 Results at the central alignment of the facade: (a) maximum out-of-plane displacement; (b) maximum drift.

As a complement to the interstory results, vertical alignments were defined. In these alignments the maximum displacements and the maximum slopes, in terms of in-plane and out-of-plane displacement, were plotted. Here, the slope is equal to the relative displacement between the node and the lower floor, divided by the relative vertical direction (Eq. (12) and Fig. 20). It is noted that when the first and the last nodes of the floor are used, the slope is equal to the typical interstory drift.

$$Slope_{Nj\,ni} = \left|\frac{u_{ni} - u_{Nj}}{h_{ni} - h_{Nj}}\right| \tag{12}$$

Figure 21 shows the maximum out-of-plane displacement of a quarter of the structure. Through this representation it is observed that in the facades the displacements increase from the border to the center of the wall and the maximum out-of-plane displacement take place at the 4th floor's pier (about 16 mm) and not at the top of the structure (10 mm). In the side gable walls the maximum out-of-plane displacement takes place at the top of the structure (about 32 mm) both at the border and central alignment.

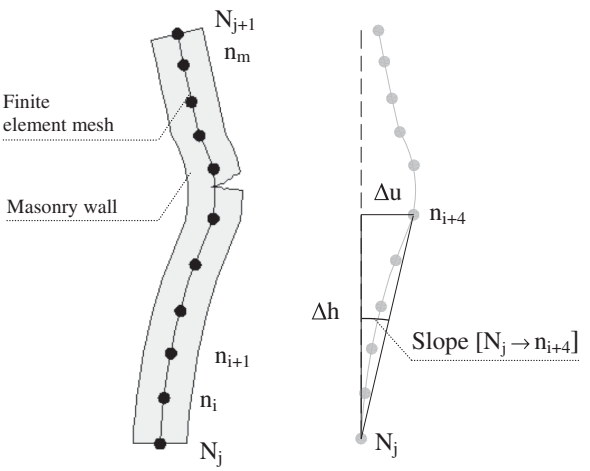

N_j is the node at the *j* floor level (j = 1,2,…4) or at the base level (j = 0)

n_i is the node *i* among floors (i = 1,…,m)

Δu is the out-of-plane relative displacement $\Delta u = u_{nj+4} - u_{Nj}$

Δh is the relative height $\Delta h = h_{nj+4} - h_{Nj}$

FIGURE 20 Definition of out-of-plane slope.

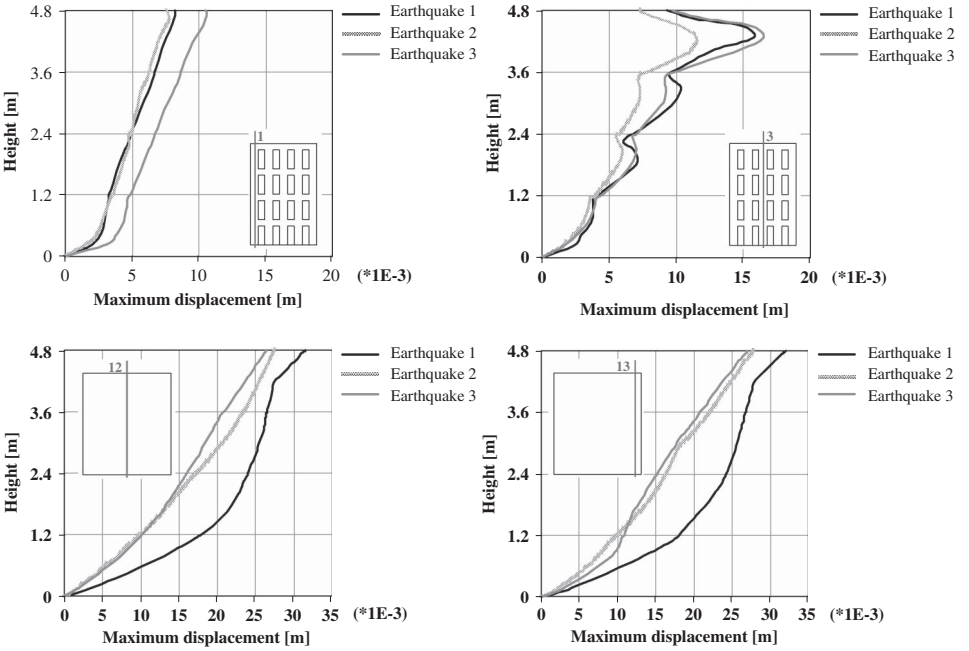

FIGURE 21 Maximum out-of-plane displacement.

The plot of the maximum out-of-plane slope (Fig. 22) indicates that the central 4th floor's piers and the base of the structure are the zones of largest damage (slopes higher than 1%), in agreement with the crack patterns of the dynamic analysis.

The in-plane results indicate that the maximum displacement of the facades is equal to 32 mm (top of the structure), without meaningful differences between the central and the border alignments. In the side-walls the maximum displacement is about 11 mm (top of the structure) and no meaningful differences were found between the central and

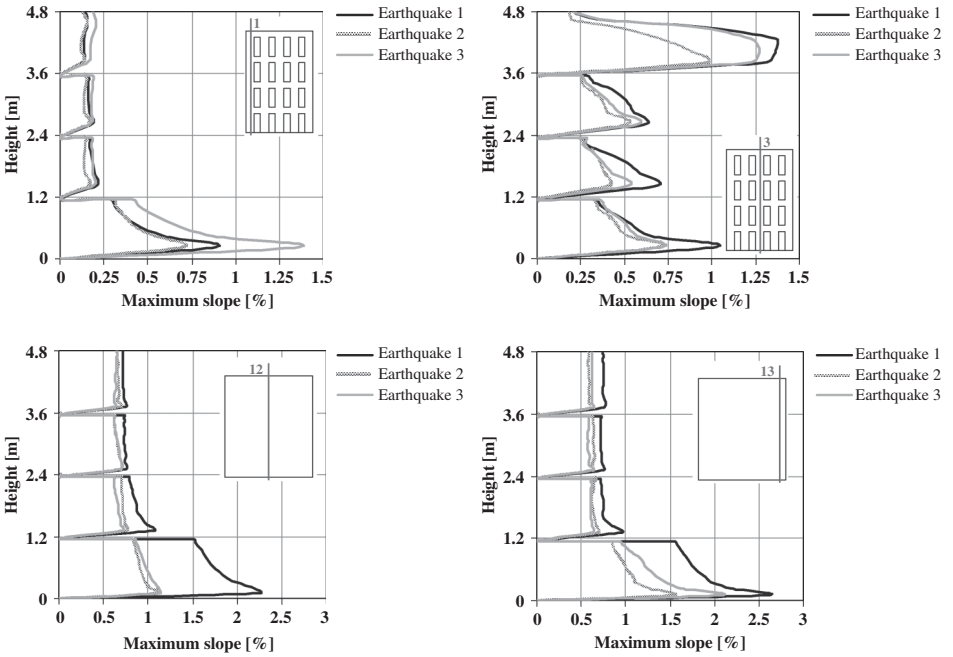

FIGURE 22 Maximum out-of-plane slope.

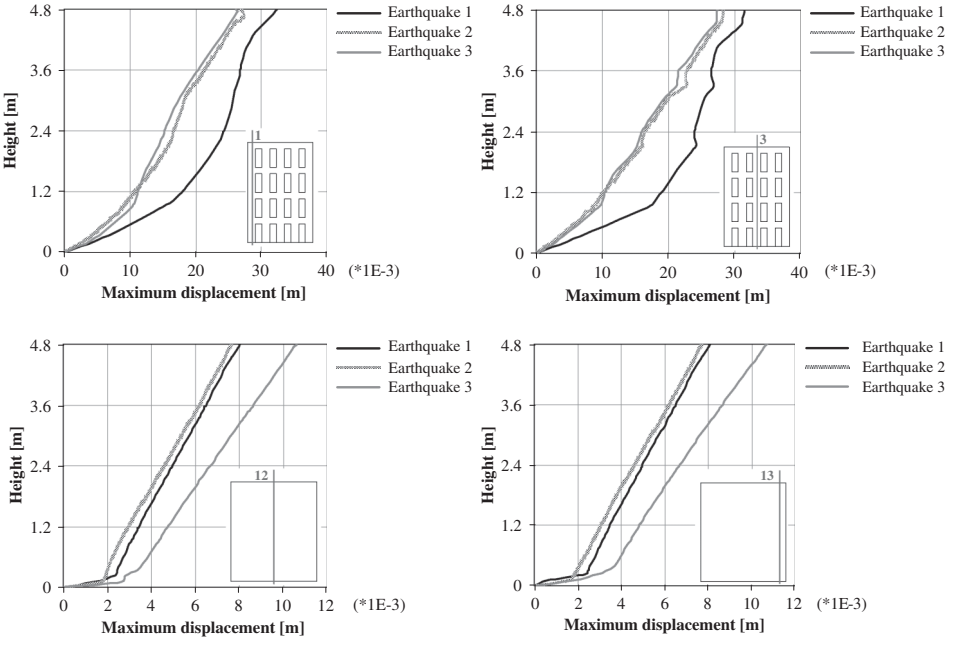

FIGURE 23 Maximum in-plane displacement.

the border alignments. However, the sharp increase of the displacement at the base is highlighted on the plots (Fig. 23).

Concerning the maximum in-plane slope (Fig. 24), it is verified that in the facades the maximum values occur at the base of the structure (larger than 2%) and in the 2nd to

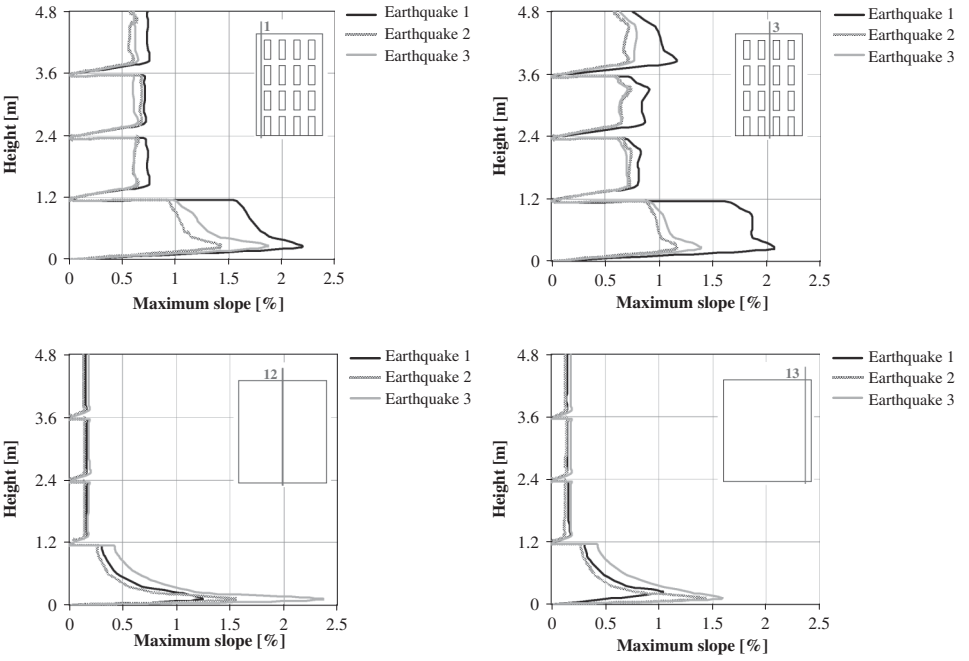

FIGURE 24 Maximum in-plane slope.

4th floors the maximum slope is about 0.75%. In the side-walls the maximum slope takes place also at the base of the structure (larger than 1.5%). However, in the 2nd–4th floors of the side-walls the in-plane slope is only about 0.2% (walls without openings).

Through the combined effects of in-plane and out-of-plane results, it is concluded that the side-walls present a damage concentration at the base of the structure. But the facades are the most vulnerable walls, being possible to identify damage at the base, cracking around the corners of the opening corners and out-of-plane collapse of the 4th floor's piers. Thus, the use of the displacements and the slopes, using the nodes of the finite element mesh, is in agreement with the crack patterns, representing good indicators of damage.

7. Conclusions

Through a nonlinear time history analysis it was observed that the buildings of "gaioleiro" type with appropriate floor-wall connection, under seismic action (Lisbon zone and soil of the type A) are in the limit of their loading capacity according to the earthquake action proposed in the new Eurocode 8 National Annex. Therefore, it seems that a strong floor-wall connection is not enough to guarantee the good performance of the building under seismic load, due to the floors flexibility.

The "gaioleiro" buildings present the typical collapse of masonry buildings including: (a) cracking around the corners of the openings; (b) out-of-plane collapse (4th floor's piers). The displacements at floor levels and the interstorey drifts are not appropriate to detect the damaged zones of the structure, as the maximum amplitudes of the response do not occur at floor levels. The plot of displacements and slope, using the nodes of the finite elements mesh into vertical alignments seem good indicators of damage. Thus,

the evaluation of the structural behavior of masonry buildings should take into account points in between floors, namely in the upper floors.

With respect to pushover analyses (proportional to the mass or to the 1st mode), it was concluded that these do not simulate correctly the failure mode of the structure, meaning that vibration modes with higher frequencies have a significant contribution to the behavior. The pushover analysis proportional to the 1st mode shape performed better in terms of load-displacement diagram than the pushover analysis proportional to the mass, simulating correctly the in-plane behavior.

In an attempt to explore the nonlinear static analyses proportional to the 1st mode shape, an adaptive pushover analysis was carried out, in which the load distribution was updated as a function of the existing damage. This analysis did not provide any improvement in terms of load-displacement diagrams or failure mechanisms.

The news versions of nonlinear static analyses (for instance the Modal Pushover Analysis introduced by Chopra and Goel (2002) or the Adaptive Capacity Spectrum Method recently proposed by Casarotti and Pinho (2007)) include the effects of higher modes of vibration and should be tested for the ''Gaioleiro'' buildings in some future work.

Even if the structure analyzed presents regularity in plan and in elevation, the flexible floors are most likely the reason for the deficient performance of the pushover analysis.

Acknowledgments

The authors are grateful to the National Laboratory of Civil Engineering for providing the experimental data for the shaking table tests. The present work is partly funded by FCT (Portuguese Foundation for Science and Technology), through project POCI/ECM/61671/2004, ''Seismic vulnerability reduction of old masonry buildings'' and PhD grant SFRH/BD/32190/2006.

References

Barbat, A. H., Pujades, L. G., and Lantada, N. [2006] ''Performance of buildings under earthquakes in Barcelona, Spain,'' *Computer-Aided Civil and Infrastructure Engineering* **21**, 573–593.

Benedetti D., Carydis P., and Pezzoli P. [1998] ''Shaking table tests on 24 simple masonry buildings,'' *Earthquake Engineering and Structural Dynamics* **27**, 67–90.

Candeias, P., Costa, A. C., and Coelho, E. [2004] ''Shaking table tests of 1:3 reduced scale models of four story unreinforced masonry buildings,'' *Proc. of the 13th World Conference on Earthquake Engineering*, Vancouver, Canada.

Carvalho, E. C. [1998] ''Seismic testing of structures,'' *Proc. of the 11th European Conference on Earthquake*, Paris, France. Rotterdam: AA Balkema.

Casarotti, C. and Pinho, R. [2007] ''An adaptive spectrum method for assessment of bridges subjected to earthquake action,'' *Bulletin of Earthquake Engineering* **3**, 377–390.

Cervera, M., Oliver, J., and Faria R. [1995] ''Seismic evaluation of concrete dams via continuum damage models,'' *Earthquake Engineering and Structural Dynamics* **24**, 1225–1245.

Chopra, A. K. [2000] *Dynamic of Structures – Theory and Applications to Earthquake Engineering*, Prentice Hall, Englewood Cliffs, NJ.

Chopra, A K. and Goel, R. K. [2002] ''A modal pushover analysis procedure for estimating seismic demands for buildings,'' *Earthquake Engineering and Structural Dynamics* **21**, 561–582.

DIANA [2005] *DIsplacement method ANAlyser*. Release 9.1, Cd-rom, Netherlands.

Douglas, B. M. and Reid, W. H. [1982] ''Dynamic tests and system identification of bridges,'' *Structural Division*, ASCE **108**, 2295–2313.

EN 1998-1 [2004] *Eurocode 8: Design of structures for earthquake resistance – General rules, seismic actions and rules for buildings*.

GAMS [1998] The General Algebraic Modeling System, CD-Rom, GAMS Development GAMS Publisher GAMS Development Corporation; Washington, USA.

Gelfi, P. [2006] *SIMQKE_GR – Artificial earthquakes compatible with response spectra*, University of Brescia, Italy.

Gulkan, P., Aschheim, M., and Spence, R. [2002] "Reinforced concrete frame buildings with masonry infills," World Housing Encyclopedia, Housing report: 64. Available from www.world-housing.net.

Mendes, N. and Lourenço, P. B. [2008] "Reduction of the seismic vulnerability of ancient buildings," Activity report of project POCI/ECM/61671/2004, FCT. (in Portuguese). Available from www.civil.uminho.pt/masonry.

Oliveira, D. V. [2004] "Reduction of the risk seismic and implications in the real state," *Proc. of the 6th National Congress of Seismology and Earthquake Engineering 2004*, Special session (In Portuguese). Available from www.civil.uminho.pt/masonry.

Pinho, F. F. [2000] *Walls from ancient Portuguese buildings*, "Edifícios," n 8, LNEC (In Portuguese).

Ramos, L. F. and Lourenço, P. B. [2004] "Advanced numerical analysis of historical centers: A case study in Lisbon," *Engineering Structures* **26**, 1295–1310.

RSA [1984] *Safety and Actions for Building and Bridge Structures*, Portuguese code (in Portuguese).

Seismosoft [2004] *SeismoSignal – A computer program for signal processing of strong-motion data*.

SPES and GEOeRPA [2001] "Reducing the seismic vulnerability of the building stock," Available from http://www.spes-sismica.org/.

Viviane W. [2007] "Mitigation of pounding between adjacent buildings in earthquake situations," LESSLOSS final workshop, Sub-project 7 - Vulnerability reduction in structures.